HiSST: 3rd International Conference on
High-Speed Vehicle Science & Technology
14–19 April 2024, Busan, Korea

# Sensitivity Derivatives of a Low-Order Integrated Scramjet Propulsion Model for Gradient-Based Co-Design MDAO

*Amir Mittelman*[1], *Kieran Mackle*[1], *Ingo Jahn*[2], *and Rowan Gollan*[1]

## Abstract

Scramjet-propelled hypersonic vehicles hold vast promise in improving operational flexibility while also reducing the cost of access to space launch systems. However, the highly coupled nature of their components and subsystems makes the design and optimization of such vehicles challenging. To address such cross-coupled, large-scale design problems, computationally efficient tools and a modular approach are needed for the evaluation of the system objectives (performance) and design sensitives (relationship between performance and design variables). In this work, we adopted the modular design framework approach and demonstrated the feasibility of efficiently yet accurately calculating the vehicle sensitivity matrix by combining quick-to-compute component-level partial derivatives. The propulsion system, up to the combustor exit, for both on- and off-design flight conditions is modeled using the newly developed tool `HyperPro`. An isentropic sensitivity calculation was added into the aerodynamic solver `PySAGAS` for nozzle performance analysis. The system level performance and sensitivity calculations were verified by comparison to an inviscid CFD solver - this showed good accuracy of the modular and isentropic approach. The demonstrated effectiveness and flexibility confirm the potential of this approach for Multi-disciplinary Design Analysis and Optimization (MDAO) when applied to complex aerodynamic and fluid dynamic systems such as scramjet-propelled hypersonic platforms.

**Keywords:** *Vehicle Design, Scramjet, Hypersonics*

## Nomenclature

| | |
|---|---|
| $OPM$ | Oblique Prandtl-Meyer |
| $P-M$ | Prandtl-Meyer |
| $STA$ | Stream Thrust Average |
| $\Psi$ | $1+\frac{\gamma+1}{2}M^2$ |
| $\vec{\theta}$ | Vector of design variables |
| $\vec{u}$ | Vector of control variable |
| $\beta$ | $\sqrt{M^2-1}$ |
| $\nu$ | Prandtl-Meyer angle [deg] |
| $\zeta$ | Design variable angle [deg] |
| $f$ | Integral of flux across specific plane |
| $g$ | Gas flow state - (M, P, T, $\alpha$, $\gamma$) |

**Subscript**

| | |
|---|---|
| $a$ | Axial direction |
| $energy$ | Energy flux |
| $mass$ | Mass flux |
| $mom$ | Momentum flux |
| $n$ | Normal direction |

**Superscript**

| | |
|---|---|
| Ⓒ | Cowl intake entrance plane |
| Ⓔ | Combustion chamber exit plane |
| Ⓕ | Free-stream |
| Ⓘ | Engine throat plane |
| $aero$ | airframe aerodynamics |
| $combustor$ | Combustion chamber |
| $cowl$ | Cowl intake (internal inlet) |
| $inlet$ | External inlet |
| $nozzle$ | External expansion nozzle |

[1]*School of Mechanical and Mining Engineering, Center for Hypersonics, University of Queensland, St. Lucia QLD 4072, Australia*
[2]*Institute for Advanced Engineering and Space Sciences, Springfield Campus, The University of Southern Queensland, Toowoomba, QLD, 4350, Australia*

## 1. Introduction

The conceptual design of hypersonic vehicles presents a formidable design challenge. The tight coupling of subsystems and the multitude of intricately coupled physical phenomena that govern their flight dynamics, aerodynamics, thermodynamics, and structural response necessitate a holistic treatment of the entire system. Especially so, when designing a scramjet-propelled hypersonic vehicle. Here the propulsion system characteristics are one of the main drivers of the airframe design and thus should be introduced alongside aerodynamic optimization. Including trajectory optimization in the vehicle design process (Co-design) holds even greater merit as the optimization problem effectively becomes a multi-point optimization providing mission-level performance objectives to be included in the decision-making process. A wide variety of MDAO techniques and frameworks have been explored in recent years [1]–[4], as they directly address the complexities inherent to hypersonic vehicle design by concurrently considering multiple interdependent disciplines and optimizing the design variables to meet the performance requirements.

As the design grows in complexity, more disciplines become involved in the optimization process, posing several challenges. First, the design space rapidly expands to include an ever-growing number of design variables. Second, different subsystems require different simulation approaches and tools, so using a single 'one size fits all' simulation framework can be highly limiting.

Gradient-based optimization algorithms are one way to work in high-dimensional design spaces efficiently [5] and therefore are desired for the Co-design system-level optimization process. An underlying modular design framework comprised of component-level analysis tools of different complexity, computational efficiency, and accuracy is suggested as the basis of such an optimization framework. The modular approach may significantly improve the computational efficiency of the analysis tools, while simultaneously "opening a window" into the system's individual component performance sensitivities. Both qualities are well appreciated when solving Co-design MDAO problems over a large number of design variables. Computational efficiency will arise from adjusting the computational cost of each individual analysis tool according to its impact on the system performance index, and from utilizing the chain rule to combine cheap(er) to compute partial derivatives rather than differentiating the entire vehicle model. Additionally, the modular approach allows cross-component sensitivities to be shared easily, thus enabling system-level insights at the component-level design.

In this work, we demonstrate that the system performance and design sensitivities of a conceptual 2-D hypersonic air breather can be calculated accurately and efficiently using a modular approach. The conceptual 2-D scramjet-propelled vehicle is analyzed by combining an oblique shock forebody inlet and cowl model, and a 1-D engine model with `PySAGAS` [6] for airframe aerodynamics and nozzle analysis. Comparison to partial and full system simulations using the 2-D inviscid flow solver `Puffin` [7] show that both the modular approach and the approximate methods yield accurate results.

## 2. Background

The current paper focuses on demonstrating the ability to efficiently and accurately calculate the performance and design sensitivities (gradients) of an integrated low-order scramjet model, for future use as the basis of an MDAO framework. Therefore, the introduction of four topics should be made - Gradient-based MDAO, methods for efficient gradient calculation, scramjet propulsion integration, and scramjet models.

### 2.1. Gradient-based MDAO

In hypersonic vehicle optimization problems, gradient-free algorithms are often used [2], [3], [8], [9], presumably because of the complexity of generating the Jacobian matrix. However, the use of gradient-free optimization algorithms can highly restrict the scale of the problem that can be solved, that is the number of design variables allowed is limited. Gradient-based algorithms reduce the number of design iterations required for convergence by exploiting the objective function sensitivities (gradient) as well as the objective function value. This is significant when optimizing over a large number of design variables [5], as often required in hypersonic MDAO problems. Recent demonstrations of gradient-based MDAO include works by Mackle *et al.* [6], [10], which efficiently optimized a hypersonic glider for maximum Lift to Drag ratio and maximum range respectively.

### 2.2. Methods for efficient gradient calculation

Efficient methods of numeric differentiation such as Automatic Differentiation (AD) [11], and Adjoint [4], [12] have been adopted in various aerospace optimization tools. Although extremely efficient and providing high-fidelity results, the development and adaptation of a design tool (i.e. CFD solver) to the use of such methods require lengthy and expensive development, highly proficient users, and relatively powerful computational capability. Therefore, calculating the system derivatives in their entirety is still a computationally costly and slow process. Chain-ruling a series of localized partial derivative matrices (either of high- or low-order), can efficiently provide an approximation

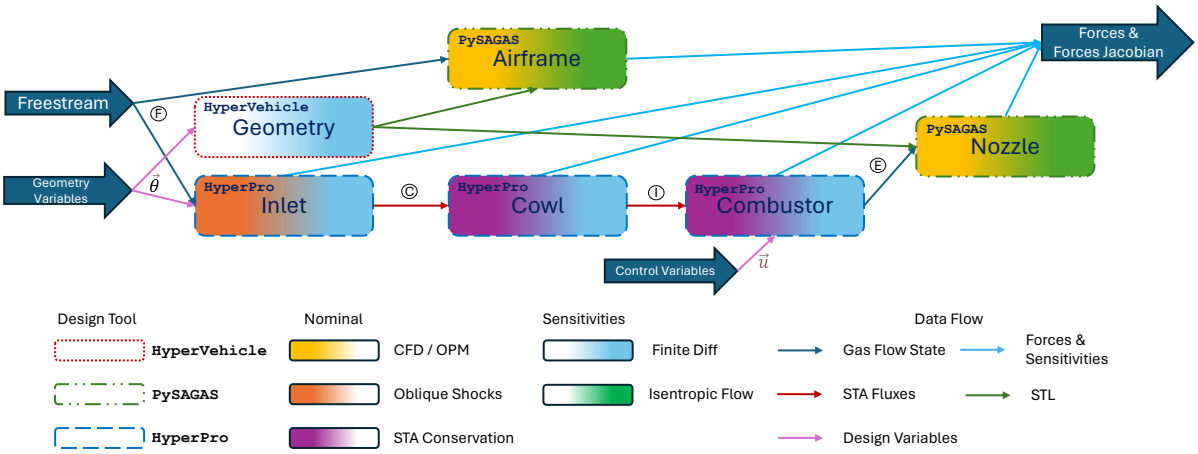


**Fig 1.** Analysis flow-chart for calculation of forces and sensitivities.

to the required Jacobian matrix. Mackle *et al.*[6] demonstrated the effectiveness of applying a modular approach combined with low-order localized analytical sensitivity calculation.

### 2.3. Scramjet propulsion integration

Unlike low-speed propulsion systems, a scramjet engine is highly integrated into the vehicle's airframe [13]. At the fore end of the vehicle, the oblique shock waves generated from the nose, together with the forebody function as an external compression inlet. At the aft end of the vehicle, the high expansion ratio of the exhaust gasses dictates that most of the vehicle's aft body volume will be devoted to the nozzle geometry [14]. This, combined with the most common asymmetric scramjet flow path geometry, results in the fact that the lift force and pitching moment generated by the propulsion system may be on the order of magnitude of the airframe aerodynamic forces [3]. To attain maximum system performance, it is critical to consider the aerodynamic forces and energy transfers at the system level to capture the intrinsic close coupling between aerodynamics and propulsion [15].

### 2.4. Scramjet engine models

Scramjet engine models can be sub-categorized into three groups: First, the high-end tools comprise high-fidelity CFD simulations capable of simultaneously solving the fluid mechanic characteristics along with finite rate chemical reactions (combustion) [16], [17]. This group is rarely included in optimization problems as the computation cost renders their usage intractable. Next, the high-fidelity but restricted tools include surrogate models constructed from multiple high-fidelity simulations or experimental results. Surrogate models can quickly evaluate the propulsion system characteristics and are easily and efficiently differentiated using finite differences. These models are widely used in optimization, as they are supported by high-fidelity results and low real-time computational burden [3], [8]. However, the underlying databases used to generate the surrogate model are expensive to generate and limited to the design variables and flight conditions covered during generation. Therefore these models lack robustness to changes in design variables and flight conditions. Finally, there are fast and flexible low-fidelity numeric or analytic design tools [18], [19]. These methods are widely used in hypersonic air-breathing propulsion analysis and vehicle optimization [20], however, they should only be used where the sensitivity to error is low, such as during the conceptual design phase [21].

## 3. Methodology

The process of calculating the vehicle's aerodynamic and propulsive characteristics, alongside their respective sensitivities is presented. A modular approach combining individual disciplinary and physical component models allows for easy integration of off-the-shelf analysis tools of different fidelity levels and computational complexity. Additionally, the modular approach allows sub-system partial derivatives, that are computationally cheaper to be combined using the chain rule, rather than calculating full system derivatives. The vehicle analysis tool developed combines several models, each providing the nominal component characteristics and their partial derivative to geometry design variables and control variables.

Fig. 1 exhibits a color-coded design tool flow-chart. The outline of each box represents the three custom-developed Python packages, while the filling colors represent the nominal characteristic (performance) calculation method (left) and the sensitivity calculation method (right). The interface planes between the different design tools are annotated,

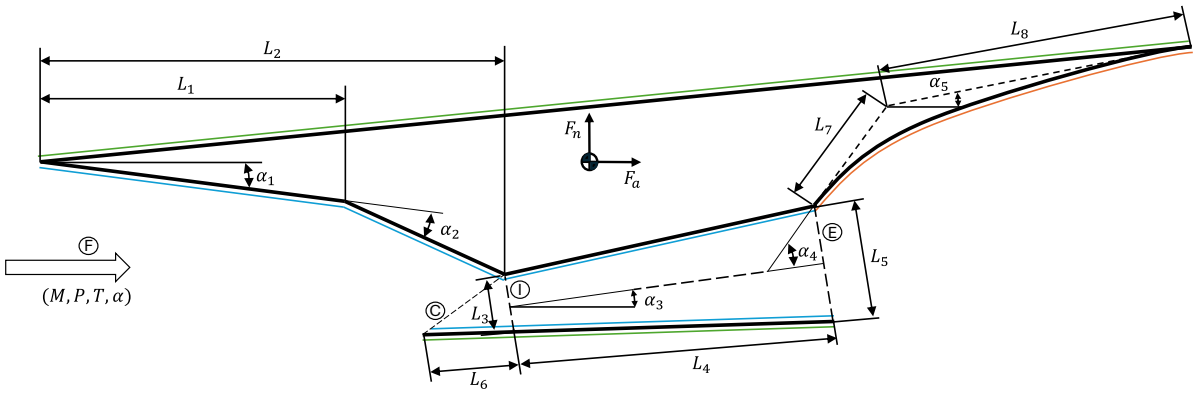


**Fig 2.** Vehicle geometry definitions. Colored surfaces indicate the model used for force/sensitivity calculation, Section 3.4. — `PySAGAS` airframe, — `PySAGAS` nozzle, — `HyperPro`

**Table 1.** Description of vehicle geometry design variables and nominal values for reference vehicle.

| Variable | Parameter | Nominal Value | Units | Description |
|---|---|---|---|---|
| $\theta_0$ | $\zeta_1$ | 3 | deg | 1st forebody ramp angle |
| $\theta_1$ | $\zeta_2$ | 5 | deg | 2nd forebody ramp angle |
| $\theta_2$ | $\zeta_3$ | 0 | deg | Engine alignment angle |
| $\theta_3$ | $\zeta_4$ | 20 | deg | Nozzle start angle |
| $\theta_4$ | $\zeta_5$ | 9.42 | deg | Nozzle aft angle |
| $\theta_5$ | $L_1$ | 1 | m | 1st forebody ramp length |
| $\theta_6$ | $L_2$ | 1.3 | m | 2nd forebody ramp length |
| $\theta_7$ | $L_3$ | 0.1 | m | Engine throat height |
| $\theta_8$ | $L_4$ | 3 | m | Engine + isolator length |
| $\theta_9$ | $\frac{L_5}{L_3}$ | 1 | - | Engine expansion ratio |
| $\theta_{10}$ | $L_6$ | 0.1 | m | Cowl lip overhang |
| $\theta_{11}$ | $L_7$ | 0.4 | m | Nozzle Bezier control point |
| $\theta_{12}$ | $L_8$ | 1.34 | m | Nozzle aft length |

and the arrow color represents the data type passed through the design framework. The geometry generation tool (`HyperVehicle`) and the external aerodynamics analysis tool (`PySAGAS`) are briefly presented in Section 3.1 and Section 3.2, respectively. The 2-D engine model `HyperPro`, developed new in this work, is described in Section 3.3. Finally, Section 3.5 describes the sensitivity evaluation approach applied to the engine and nozzle.

Both pre-existing packages were expanded in the current work, to enable the propulsion system integration into the vehicle design process. This includes the calculation of nozzle performance using the engine outflow conditions, and the calculation of analytic partial derivatives of the nozzle forces with respect to the engine outflow conditions (see Section 3.5).

### 3.1. Geometry

The vehicle geometry is defined by a set of 13 design variables provided by the user or an optimization loop. A surface mesh is generated using the Python package `HyperVehicle` [6], providing a convenient interface to the `GDTk` geometry library [22]. `HyperVehicle` is used first to generate a parametrically defined vehicle mesh, and second, to provide the sensitivities between the vehicle geometry design variables and cell area ($\frac{\partial A_i}{\partial \vec{\theta}}$) and cell normal vector ($\frac{\partial \hat{n}_i}{\partial \vec{\theta}}$). A schematic of the vehicle geometry is shown in Fig. 2, defining all geometry design variables. A list of all geometry design variables along with their nominal values used in the current work is provided in Table 1. As `HyperVehicle` generates 3-D geometries, for the current 2-D study, the 2-D geometry was extruded to have unit width.

### 3.2. Airframe Aerodynamics

The airframe aerodynamic characteristics (green and orange lines in Fig. 2) are calculated using the Python package `PySAGAS` [6]. `PySAGAS` includes the low fidelity Oblique-Prandtl–Meyer (OPM) solver, which combines oblique shock and Prandtl-Meyer (P-M) relations to calculate vehicle surface flow states. Comparison of the OPM solver with a higher-fidelity CFD simulation (`Cart3D`) showed reasonable agreement for a wave-rider configuration [10]. `PySAGAS` also provides sensitivities of aerodynamic forces and moments to geometrical design variables by applying asymptotic compressible flow relations [6].

### 3.3. Forebody and Engine

The propulsion system performance is calculated using the Python package `HyperPro` [23]. The engine is subdivided into four components: external forebody compression inlet (Inlet), internal compression inlet (Cowl intake), isolator duct and combustion chamber (Combustor), and external expansion nozzle (Nozzle). `HyperPro` analytically analyzes the 2-D flow for the inlet and cowl. This is then coupled to a quasi-1-D isolator and combustor model. The nozzle section of the propulsion system is analyzed by `PySAGAS` utilizing the outflow condition from the combustor. Additionally, `HyperPro` provides the sensitivities matrix of the propulsion system to the vehicle design variables and engine control variables.

The Stream-Thrust-Average (STA) fluxes, $\vec{f}$, are used for the flow interface between the different components of the engine flow path (Ⓒ for Inlet-Cowl interface, and Ⓘ for Cowl-Combustor interface). The STA fluxes are calculated by integrating Eq. 1 across a given duct plane to convert a 2-D (or 3-D) flow to an equivalent 1-D representation [24].

$$f_{mass} = \int_S [\rho(\vec{V} \cdot \hat{n})] dS \tag{1a}$$

$$\vec{f}_{mom} = \int_S [\rho(\vec{V} \cdot \hat{n})\vec{V} + p\hat{n}] dS \tag{1b}$$

$$f_{energy} = \int_S [\rho(\vec{V} \cdot \hat{n}) h_0] dS \tag{1c}$$

$$h_0 = C_p T + \frac{|\vec{V}|^2}{2} \tag{2}$$

The interface planes Ⓒ, Ⓘ, and Ⓔ locations are defined in Fig. 2.

#### *3.3.1. Inlet*

The external forebody inlet model calculates the STA of the mass, momentum, and energy fluxes entering the engine duct. A series of oblique shocks, forming over the forebody ramps are solved [13] to provide the flow conditions across the cowl intake entrance plane Ⓒ.

For optimal performance, the forebody and cowl are designed such that shocks from both ramps impinge on the cowl lip. The resulting shock-on-lip conditions are optimal as they avoid spillage drag, which arises from flow being compressed by the forebody shock wave(s) but not being ingested into the engine duct. However, vehicles with a fixed geometry will have to operate at off-design conditions when the flight angle of attack or Mach number moves away from the design point. To analyze external inlet (forebody) performance, four cases as shown in Fig. 3 are considered:

(a) Both shocks spilling (Fig. 3a) - here the flow state 2 defines the flow entering the inlet.

(b) One shock ingested - once a shock crosses plane Ⓒ, it is ingested into the engine duct (Fig. 3b). At this operating condition, two flow states enter the engine duct. The STA fluxes at plane Ⓒ are obtained by integrating Eq. 1 from the cowl lip to the second ramp shock using the free-stream flow conditions Ⓕ, and then from the shock to the body using flow state 2.

(c) Two shocks ingested - Fig. 3c represents the case where both the first and second ramp shock waves are ingested into the engine duct. Here the free-stream flow Ⓕ as well as flow states 1 and 2 are used to calculate the STA fluxes.

(d) Shock-shock interaction - Fig. 3d depicts a shock-shock interaction case, where the two ramp shock waves meet upstream of the cowl intake. This will form two new shock waves, and a slip line dividing the different flow states downstream of the interaction point. This is an extremely unwanted flow pattern, and will preferably be avoided for a well-designed inlet. Currently, the following simple assumption is made: the first ramp

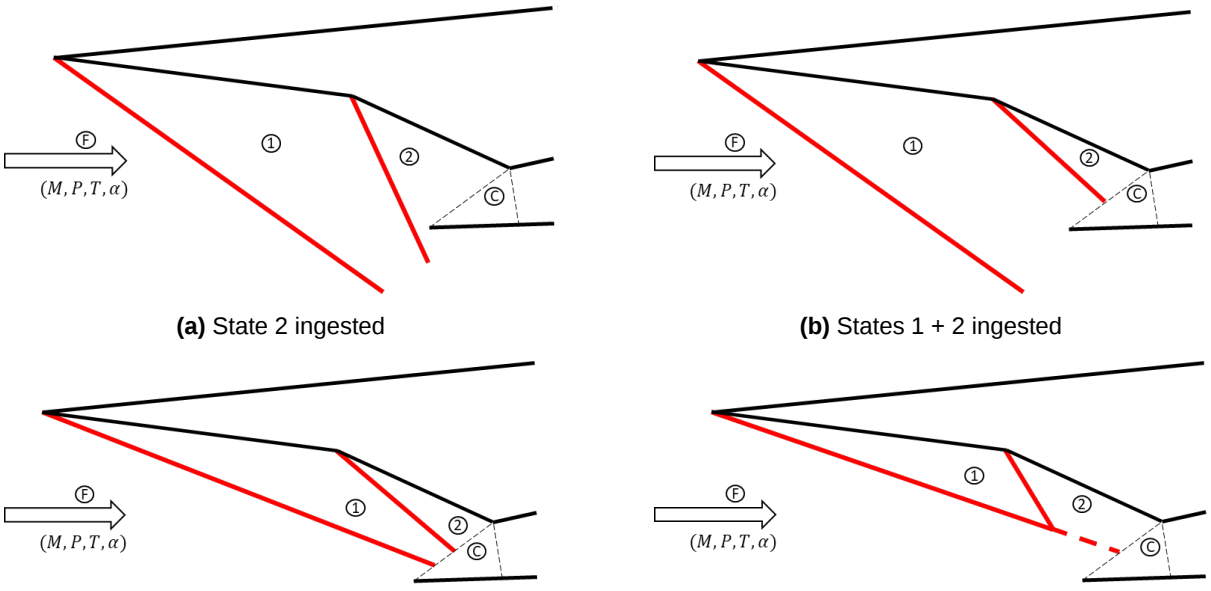


**(a)** State 2 ingested

**(b)** States 1 + 2 ingested

**(c)** States F + 1 + 2 ingested

**(d)** States F + 2 ingested

**Fig 3.** Schematic showing four cases considered for modeling Inlet off-design operation.

shock wave is extended and we assume that free-stream flow Ⓕ along with flow state 2 are ingested into the engine duct. A more detailed model may be introduced in future work as required by vehicle and trajectory optimization results.

Outputs from the inlet model include the STA fluxes across plane Ⓒ - $(f^C_{mass},\ \vec{f}^C_{mom},\ f^C_{energy})$, and the forces acting on the external inlet ramp surfaces $(F^{inlet}_a,\ F^{inlet}_n)$

### *3.3.2. Cowl Intake*

After entering the engine duct, a series of oblique shock waves ("shock train") forms starting at the cowl leading edge and continuing throughout the length of the isolator. The purpose of the shock train is to further compress the incoming flow while rotating it to be parallel to the engine center line, $\hat{n}^I$. The isolator serves also as a barrier between the inlet and the combustion chamber damping unwanted flow phenomena crossing from one to the other. `HyperPro` models this process by considering the conservation of mass, momentum, and energy to create a robust approach that can cope with off-design conditions. The conservation equations are solved between the cowl intake plane Ⓒ and the engine throat line Ⓘ. A force, acting perpendicular to the engine center-line, $\vec{F}^{cowl}$ is added to the momentum equations, to accommodate the change in flow direction and to capture associated forces acting on the inside cowl surface.

$$f^I_{mass} = f^C_{mass} \tag{3a}$$
$$\vec{f}^I_{mom} = \vec{f}^C_{mom} + \vec{F}^{cowl} \tag{3b}$$
$$f^I_{energy} = f^C_{energy} \tag{3c}$$

$$\vec{F}^{cowl} = \vec{f}^C_{mom} - \left(\vec{f}^C_{mom} \cdot \hat{n}^I\right)\hat{n}^I \tag{4}$$

The cowl intake model outputs the STA fluxes across plane Ⓘ - $(f^I_{mass},\ \vec{f}^I_{mom},\ f^I_{energy})$, and the forces acting on the lower duct surface $\left(F^{cowl}_a,\ F^{cowl}_n\right)$

#### *3.3.3. Combustor*

In lieu of a full chemistry and combustion model, the combustion process is modeled by introducing mass flow rate, momentum, or heat source terms into the flow conservation equations. The correct choice of these source terms and adjustment of the ratio of specific heats, $\gamma$ at the outlet is a way to replicate a real combustor. The source terms can be defined by the user or an optimization loop and serve as the engine's control variables. The control variables and their nominal values are presented in Table 2. Axial force may be generated for a diverging area duct $\theta_9 = \frac{L_5}{L_3} > 1$.

**Table 2.** Propulsion system control variables.

| Variable | Parameter | Nominal Value | Units | Description |
|---|---|---|---|---|
| $u_1$ | $\Delta f_{mass}$ | $0$ | kg/s | Mass flux source |
| $u_2$ | $\Delta \vec{f}_{mom}$ | $\vec{0}$ | N | Momentum flux source |
| $u_3$ | $\Delta f_{energy}$ | $10^7$ | J/s | Energy flux (heat addition) source |

$$f^E_{mass} = f^I_{mass} + \Delta f_{mass} \tag{5a}$$

$$\vec{f}^E_{mom} + \vec{F}^{combustor} = \vec{f}^I_{mom} + \Delta \vec{f}_{mom} \tag{5b}$$

$$f^E_{energy} = f^I_{energy} + \Delta f_{energy} \tag{5c}$$

$$\vec{F}^{combustor} = \left[ L_3 \left( \frac{L_5}{L_3} - 1 \right) \frac{P^E - P^I}{2} \right] \hat{n}^I \tag{6}$$

Note that $\hat{n}^I$ is the unit vector aligned with the combustor center line. The resulting STA fluxes at the engine exit plane (E) are used to estimate the engine's outflow state. This is done by inverting and iteratively solving the STA equations (Eq. 1) for the flow conditions - $(M^E,\ P^E,\ T^E)$.

The outputs of the combustor model are the force acting on the diverging duct, $\vec{F}^{combustor}$, and the engine's outflow state $(M^E,\ P^E,\ T^E,\ \alpha^E,\ \gamma^E)$, where $\alpha^E = \zeta_3$ is the engine alignment angle and $\gamma^E = \gamma^F$ (no change in flow specific heat ratio is currently included).

### 3.4. Force Book-Keeping

The total vehicle forces are calculated by summing all component contributions:

$$\vec{F} = \underbrace{\vec{F}^{aero}}_{I} + \Big[ \underbrace{\vec{F}^{inlet} + \vec{F}^{cowl} + \vec{F}^{combustor}}_{II} \Big] + \underbrace{\vec{F}^{nozzle}}_{III} \tag{7}$$

The different contributions are highlighted in Fig. 2. $I$ - green - airframe aerodynamics (Section 3.2), $II$ - blue - inlet, cowl and combustor (Section 3.3), and $III$ - red - nozzle flow (Section 3.2 using the engine outflow conditions)

### 3.5. Sensitivities

The goal of the sensitivity analysis is to obtain the system Jacobian matrix - this matrix contains partial derivatives of model output to system input variables. Calculating the full derivatives of the aerodynamic and propulsive forces to the vehicle design variables can prove computationally intractable, especially when optimizing for a large number of design variables. However, calculating the partial derivatives of different components is often much simpler. In the present study, the Jacobian is the sensitivity of forces to all design variables $J = \left[ \frac{\partial \vec{F}}{\partial \vec{\theta}} \right]$, where $\vec{F}$ is the force vector, and $\vec{\theta}$ combines both geometry design variables and control variables. The vehicle Jacobian matrix is derived by differentiating the Eq. 7.

$$J = \frac{d\vec{F}}{d\vec{\theta}} = \underbrace{\frac{d\vec{F}^{aero}}{d\vec{\theta}}}_{I} + \Big[ \underbrace{\frac{d\vec{F}^{inlet}}{d\vec{\theta}} + \frac{d\vec{F}^{cowl}}{d\vec{\theta}} + \frac{d\vec{F}^{combustor}}{d\vec{\theta}}}_{II} \Big] + \underbrace{\frac{d\vec{F}^{nozzle}}{d\vec{\theta}}}_{III} \tag{8}$$

The airframe aerodynamic sensitivity matrix ($I$ in Eq. 8) is calculated using the mesh finite differences sensitivities and Van-Dyke's method for each cell's pressure sensitivity, $\frac{\partial P_i}{d\theta_j}$ as explained in detail in Mackle ***et al.***[6].

$$\frac{d\vec{F}^{aero}}{d\theta_j} = \sum_{i=0}^{N} \Bigg[ \underbrace{\frac{\partial P_i}{\partial \theta_j} A_i(\theta_j)\, \hat{n}_i(\theta_j)}_{\text{pressure sensitivity}} + \underbrace{P_i(\theta_j)\, \frac{\partial A_i}{\partial \theta_j}\, \hat{n}_i(\theta_j)}_{\text{area sensitivity}} + \underbrace{P_i(\theta_j)\, A_i(\theta_j)\, \frac{\partial \hat{n}_i}{\partial \theta_j}}_{\text{normal sensitivity}} \Bigg], \quad j = 1, \ldots, M \tag{9}$$

Where $P$, $A$, and $\hat{n}$ are the cell's pressure, area, and normal vector, respectively. $N$ is the number of cells in the mesh, and $M$ is the number of design variables.

The partial derivatives of the engine model ($II$ in Eq. 8) are calculated in `HyperPro` by finite differencing, and chain ruled to derive the force sensitivity alongside the engine outflow sensitivity

$$\frac{d\vec{F}^{inlet}}{d\vec{\theta}} = \frac{\partial \vec{F}^{inlet}}{\partial \vec{\theta}} \tag{10a}$$

$$\frac{d\vec{F}^{cowl}}{d\vec{\theta}} = \frac{\partial \vec{F}^{cowl}}{\partial \vec{\theta}} + \frac{\partial \vec{F}^{cowl}}{\partial \vec{f}^{C}} \frac{\partial \vec{f}^{C}}{\partial \vec{\theta}} \tag{10b}$$

$$\frac{d\vec{F}^{combustor}}{d\vec{\theta}} = \frac{\partial \vec{F}^{combustor}}{\partial \vec{\theta}} + \frac{\partial \vec{F}^{combustor}}{\partial \vec{f}^{I}} \left[ \frac{\partial \vec{f}^{I}}{\partial \vec{\theta}} + \frac{\partial \vec{f}^{I}}{\partial \vec{f}^{C}} \frac{\partial \vec{f}^{C}}{\partial \vec{\theta}} \right] \tag{10c}$$

$$\frac{d\vec{g}^{E}}{d\vec{\theta}} = \frac{\partial \vec{g}^{E}}{\partial \vec{\theta}} + \frac{\partial \vec{g}^{E}}{\partial \vec{f}_{I}} \left[ \frac{\partial \vec{f}^{I}}{\partial \vec{\theta}} + \frac{\partial \vec{f}^{I}}{\partial \vec{f}^{C}} \frac{\partial \vec{f}^{C}}{\partial \vec{\theta}} \right] \tag{10d}$$

Where $\vec{f} = (f_{mass},\, \vec{f}^{T}_{mom},\, f_{energy})$ is the STA flux vector, and $\vec{g} = (M,\, P,\, T,\, \alpha,\, \gamma)$ is the flow state vector, $\alpha$ is the flow angle relative to the reference coordinate system (angle of attack), and $\gamma$ is the specific heat ratio.

Finally, the nozzle sensitivity $\frac{d\vec{F}^{nozzle}}{d\vec{\theta}}$ ($III$ in Eq. 8) is calculated similarly as the aerodynamic forces (Eq. 9), with two extra considerations. First, the "free-stream" used for the nozzle cells is the outflow of the engine $\vec{g}^{E}$. Second, the analytical estimation of the pressure sensitivity is expanded to include the sensitivity due to changes in the flow conditions at the engine outlet (see Section 3.5.1).

#### *3.5.1. Nozzle Sensitivity*

The nozzle is assumed to be primarily dominated by supersonic expanding flow, which can be approximated as isentropic. Therefore, the Prandtl-Meyer equation ([13]) is used for the nozzle pressure sensitivities evaluation. It is worth noting that the low-order sensitivity calculation is independent of the baseline flow. Therefore, an external flow calculation (i.e. CFD simulation) may provide a higher fidelity nominal flow field, thus increasing the sensitivity matrix's accuracy as well. The partial derivative term for pressure sensitivity, $\frac{\partial P_i}{\partial \vec{\theta}} A_i\, \hat{n}_i$ in Eq. 9 is expanded and applied to the nozzle section, to include sensitivities to the combustor outflow conditions.

$$\boxed{\frac{\partial P_i}{\partial \vec{\theta}} A_i\, \hat{n}_i = \left( \frac{\partial P_i}{\partial \vec{\theta}} + \frac{\partial P_i}{\partial M^E} \frac{\partial M^E}{\partial \vec{\theta}} + \frac{\partial P_i}{\partial P^E} \frac{\partial P^E}{\partial \vec{\theta}} + \frac{\partial P_i}{\partial T^E} \frac{\partial T^E}{\partial \vec{\theta}} + \frac{\partial P_i}{\partial \alpha^E} \frac{\partial \alpha^E}{\partial \vec{\theta}} + \frac{\partial P_i}{\partial \gamma^E} \frac{\partial \gamma^E}{\partial \vec{\theta}} \right) A_i\, \hat{n}_i} \tag{11}$$

The governing isentropic (P-M) relations relevant to the nozzle sensitivity calculation method are presented for the readers' convenience (Eq. 12 through Eq. 15). The full derivation of the partial derivative in Eq. 11 is presented thereafter. Following notation custom to the P-M function, the derivation (up to an including Eq. 24) uses sub-script $1$ to denote engine outflow through the exit plane (E) (incoming flow), and uses sub-script $2$ to denote the local flow on any given nozzle cell (post-expansion).

The P-M function relates the change in Mach number in supersonic isentropic flow to a corresponding flow turning angle, $\nu$.

$$\frac{\partial \nu}{\partial M} = \frac{1}{M} \frac{\sqrt{M^2 - 1}}{1 + \frac{\gamma - 1}{2} M^2} = \frac{1}{M} \frac{\beta}{\Psi} \tag{12}$$

Where $\beta = \sqrt{M^2 - 1}$ and $\Psi = 1 + \frac{\gamma - 1}{2} M^2$. The corresponding Mach number dependency relation is derived as:

$$\frac{\partial M_2}{\partial M_1} = \frac{\partial M_2}{\partial \nu} \frac{\partial \nu}{\partial M_1} = \frac{M_2}{M_1} \frac{\beta_1}{\beta_2} \frac{\Psi_2}{\Psi_1} \tag{13}$$

Using the isentropic flow relation for stagnation pressure

$$P = P_0 \ (\Psi)^{\frac{-\gamma}{\gamma-1}} \tag{14}$$

and the conservation of stagnation pressure through an isentropic process $P_{02} = P_{01}$, the following pressure relation is realized

$$P_2 = P_1 \left(\frac{\Psi_1}{\Psi_2}\right)^{\frac{\gamma}{\gamma-1}} \tag{15}$$

All elements in Eq. 11 are provided for each cell $i$. Note partial derivatives of gas state at Ⓔ, $\vec{g}^E = \left(M^E,\ P^E,\ T^E,\ \alpha^E,\ \gamma^E\right)$ are obtained using Eq. 10d.

- $\frac{\partial P}{\partial \theta}$ - calculated using asymptotic compressible flow relations developed by Mackle ***et al***.[6] and based on Van-Dyke's second order method [25].
- $\frac{\partial P}{\partial M^E}$ - Differentiating Eq. 15 with respect to the outflow Mach number ($M_1$), while keeping in mind the cell Mach number dependency on the outflow Mach number (Eq. 13), results in the cell pressure sensitivity to the outflow Mach number:

$$\boxed{\frac{\partial P}{\partial M^E} = \frac{\partial P_2}{\partial M_1} = P_1 \gamma \left[ M_1 \frac{(\Psi_1)^{\frac{1}{\gamma-1}}}{(\Psi_2)^{\frac{\gamma}{\gamma-1}}} - M_2 \frac{(\Psi_1)^{\frac{\gamma}{\gamma-1}}}{(\Psi_2)^{\frac{2\gamma-1}{\gamma-1}}} \frac{\partial M_2}{\partial M_1} \right]} \tag{16}$$

- $\frac{\partial P}{\partial P^E}$ - The cell pressure sensitivity to engine outflow pressure change is realized by differentiating Eq. 15

$$\boxed{\frac{\partial P}{\partial P^E} = \frac{\partial P_2}{\partial P_1} = \left(\frac{\Psi_1}{\Psi_2}\right)^{\frac{\gamma}{\gamma-1}}} \tag{17}$$

- $\frac{\partial P}{\partial T^E}$ - From the isentropic relation, Eq. 14, and the P-M function, Eq. 13 it can be seen that the cell pressure is independent of the engine's outflow temperature.

$$\boxed{\frac{\partial P}{\partial T^E} = 0} \tag{18}$$

- $\frac{\partial P}{\partial \alpha^E}$ - The change in the outflow angle is similar to the change in the cell's inclination angle [6], but with an opposite sign due to the definition of a positive turning direction. In both cases, the flow turning angle change results in cell Mach number change and therefore cell pressure change.

$$\boxed{\frac{\partial P}{\partial \alpha^E} = -\frac{\partial P_2}{\partial M_2}\frac{\partial M_2}{\partial \alpha} = \frac{M_2^2}{\beta_2}\gamma\, P_2} \tag{19}$$

- $\frac{\partial P}{\partial \gamma^E}$ - The sensitivity of a nozzle cell's pressure to the change in the engine outflow specific heat ratio $\gamma$ is calculated by applying the chain rule to the isentropic pressure ratio, Eq. 15.

$$\boxed{\frac{\partial P}{\partial \gamma^E} = \frac{\partial P_2}{\partial \gamma} + \frac{\partial P_2}{\partial \nu}\frac{\partial \nu}{\partial \gamma}} \tag{20}$$

We now differentiate each term in the above expression:

$$\boxed{\begin{aligned} \frac{\partial P_2}{\partial \gamma} &= \frac{\partial}{\partial \gamma}\left[P_1 \left(\frac{\Psi_1}{\Psi_2}\right)^{\frac{\gamma}{\gamma-1}}\right] \\ &= P_1 \left(\frac{\Psi_1}{\Psi_2}\right)^{\frac{\gamma}{\gamma-1}} \left\{ \frac{\gamma}{2\Psi_1(\gamma-1)}\left[M_1^2 - M_2^2\frac{\Psi_1}{\Psi_2}\right] + \left(\frac{1}{\gamma-1} - \frac{\gamma}{(\gamma-1)^2}\right) \ln\left(\frac{\Psi_1}{\Psi_2}\right)\right\} \end{aligned}} \tag{21}$$

As mentioned above, the sensitivity to the cell's inclination angle is equal and opposite to that of the outflow angle. From Eq. 19 we get

$$\boxed{\frac{\partial P_2}{\partial \nu} = -\frac{\partial P_2}{\partial \alpha^E} = -\frac{M_2^2}{\beta_2}\gamma\, P_2} \tag{22}$$

The P-M equation expresses the flow turning angle $\nu$ to be

$$\nu(M) = \sqrt{\frac{\gamma+1}{\gamma-1}}\arctan\sqrt{\frac{\gamma-1}{\gamma+1}\beta^2} - \arctan\beta \tag{23}$$

Therefore the partial derivative is

$$\boxed{\frac{\partial\nu}{\partial\gamma} = \frac{\sqrt{\frac{\gamma+1}{\gamma+1}}\left(\frac{\beta_1}{\gamma+1}\right)^2}{\sqrt{\beta_1^2\frac{\gamma-1}{\gamma+1}}\left(\beta_1^2\frac{\gamma-1}{\gamma+1}+1\right)} - \frac{\frac{1}{\gamma-1}\arctan\sqrt{\beta_1^2\frac{\gamma-1}{\gamma+1}}}{\sqrt{\gamma^2-1}}} \tag{24}$$

## 4. Results

### 4.1. Verification

The methodology was verified using the nominal geometry (Table 1) and control (Table 2) variables. The nominal free-stream flow conditions was $g^F = (M = 6.5,\ q_{dyn} = 50\ [\text{kPA}],\ T = 288\ [\text{K}],\ \alpha = 5°,\ \gamma = 1.4)$. For verification, predictions were compared to the 2-D supersonic Euler CFD solver, `Puffin`, from the University of Queensland's `GDTk` repository [7].

#### *4.1.1. Prediction of Aerodynamic Forces*

Forces acting on the vehicle are divided into three contributions (Eq. 7).
$I$ - the vehicle airframe forces are calculated using the OPM solver option of `PySAGAS`. Detailed verification of this method is provided by Mackle ***et al.*** [10].
$II$ - the forces acting on the inlet, cowl, and combustor were calculated using `HyperPro` and are compared to `Puffin` predictions of the same vehicle segments in Table 3. Good agreement is observed. The current vehicle uses a vehicle axis-aligned constant cross-section engine, hence no axial or normal forces are generated. The combustor normal force predicted by `Puffin` is the result of the 2-D nature of the engine duct flow which is not captured in the 1-D `HyperPro` combustor model.
$III$ - the nozzle forces calculated by `PySAGAS`, using the combustor outflow conditions are presented in Table 3, and show good agreement to those calculated by the `Puffin` solver.

**Table 3.** Comparison of aerodynamics forces predicted using our methods to the `Puffin` solver for the nominal geometry (Table 1) and control (Table 2) design variables. Note: the nozzle forces were calculated by `PySAGAS` and `Puffin`

| | Inlet | | Cowl | | Combustor | | Nozzle | |
|---|---|---|---|---|---|---|---|---|
| | $F_a$ | $F_n$ | $F_a$ | $F_n$ | $F_a$ | $F_n$ | $F_a$ | $F_n$ |
| `HyperPro` [kN] | 0.696 | 8.3 | 0 | −3.1 | 0 | 0 | −4.76 | 23.35 |
| `Puffin` [kN] | 0.683 | 8.17 | 0 | −3 | 0 | 0.1 | −4.77 | 23.5 |
| Error [%] | 1.9 | 1.6 | – | 3.3 | – | – | 0.3 | 0.6 |

#### *4.1.2. Flow State*

The flow state and fluxes were calculated at the interface planes Ⓒ, ①, and Ⓔ (Fig. 2), and were compared to corresponding `Puffin` predictions. Fig. 4 presents the simulated static temperature along the engine's flow path. The cowl intake is simulated in `HyperPro` as a single point flow turn (between planes Ⓒ and ①), however, as shown in the `Puffin` simulation, the process of turning the flow actually takes place through a series of oblique shock that form within the isolator. Consequently, there is poor agreement when comparing fluxes or states at location ①. However, when comparing fluxes predicted by the 1-D model (`HyperPro`) at interface ①, to those calculated by the 2-D CFD solver at interface ①*, where the flow has become aligned, much better agreement is obtained. This is important, as it confirms that our method is accurate in capturing net forces and conserved fluxes, however, for high-fidelity engine design, airframe aerodynamics, and mass properties calculations the isolator length should be brought into account.

The equivalent flow conditions, as calculated from the 2-D CFD STA fluxes at the combustor exit plane Ⓔ, are presented alongside those calculated by the 1-D model in Table 4. The good agreement again demonstrates the capability of our approach.

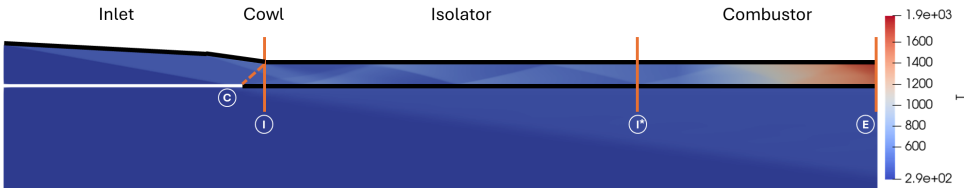


**Fig 4.** Contours of static temperature for the vehicle inlet and engine flow path - `Puffin` simulation. C - Inlet - Cowl intake interface, I - Cowl intake - Combustor interface, I* - Cowl intake - Combustor interface including isolator, E - Combustor - Nozzle interface

**Table 4.** Comparison of flow state at combustor exit. E - Combustor - Nozzle interface.

| $g^E$ | $Mach$ | $P$ [kPa] | $T$ [K] |
|---|---|---|---|
| `HyperPro` | 2.34 | 30.7 | 1683 |
| `Puffin` | 2.38 | 30.8 | 1644 |
| Error [%] | 1.4 | 0.2 | 2.4 |

#### *4.1.3. Sensitivities*

In Fig. 5, the variation in nozzle force and corresponding sensitivities to the combustor outflow conditions (terms in Eq. 11) are compared between several different calculation methods. The nozzle axial force sensitivities to Mach number, $\frac{\partial F_a}{dM^E}$ and pressure, $\frac{\partial F_a}{dP^E}$, corresponding to the slopes in Fig. 5a and Fig. 5b, respectively, are calculated using three approaches and show good agreement: (1) the sensitivity as calculated by the P-M relations (Section 3.5.1 and Eq. 10d), (2) a finite differences calculation using `PySAGAS` OPM solver (low-fidelity), (3) a finite differences calculation using the 2-D `Puffin` CFD solver. The excellent agreement confirms the accuracy of our approach. Similar verification was completed for all other terms in Eq. 11.

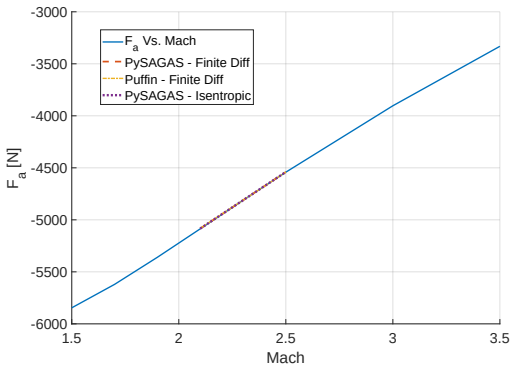


**(a)** Combustor outflow Mach number

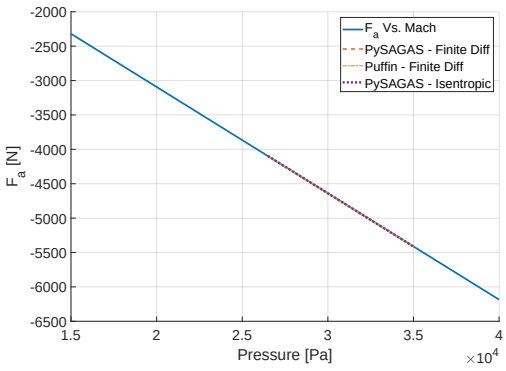


**(b)** Combustor outflow pressure

**Fig 5.** Comparison of nozzle axial force and force sensitivities to flow parameters at combustor exit. Note: lines are indistinguishable as they sit atop one another.

Table 5 compares the total vehicle force sensitivities to the design variables (Eq. 8), when calculated using two different differentiation methods, both using the `HyperPro` and `PySAGAS`: First, the modular approach that combines partial derivatives. Second, finite differencing the full tip-to-tail vehicle force calculation. The results for four representative design variables are given in Table 5. The good agreement between the two methods confirms the validity of our modular approach.

**Table 5.** Comparison of total vehicle force sensitivities calculated using `HyperPro` and `PySAGAS`: Modular partial derivative construction Vs. finite differencing calculations of tip-to-tail vehicle.

| | $\theta_1: \frac{d}{d\alpha_2}$ [N/deg] | | $\theta_5: \frac{d}{dL_1}$ [N/m] | | $\theta_7: \frac{d}{dL_3}$ [N/m] | | $\theta_{11}: \frac{d}{dL_7}$ [N/m] | |
|---|---|---|---|---|---|---|---|---|
| | $F_a$ | $F_n$ | $F_a$ | $F_n$ | $F_a$ | $F_n$ | $F_a$ | $F_n$ |
| Modular | $143.9$ | $27,254$ | $-116.8$ | $-3,876$ | $56,481$ | $-286,748$ | $-2,780$ | $5,254$ |
| Finite Diff. | $150$ | $27,325$ | $-115.6$ | $-3,858$ | $56,469$ | $-286,570$ | $-2,758$ | $5,393$ |
| Error [%] | $4$ | $0.3$ | $1.1$ | $0.5$ | $0$ | $0$ | $0.8$ | $2.6$ |

### 4.2. Discussion

The current work is a stepping stone on the path to developing a gradient-based Co-design MDAO framework for scramjet-propelled hypersonic platforms. Therefore, several key aspects of the developed tools are discussed.

#### *4.2.1. Simulation of Off-Design Operating Conditions*

When considering mission-level performance, or when solving a Co-design optimization problem, the vehicle will operate away from the nominal design point. The implication is that simulation and analysis of off-design flight conditions are an important part of the design process. Considering the forebody and engine inlet, four scenarios describing different shock geometry and ingestion were considered (Fig. 3). The STA flux calculation presented in Section 3.3.1 proved accurate in predicting the inflow conditions to the cowl and 1-D combustor models. The only exception is case (d), where the two shocks interact, which resulted in differences of up to $15\%$ in the fluxes between `HyperPro` and 2-D simulations conducted in `Puffin`. A more detailed model to treat such shock-shock interactions may be required, pending outcomes from the optimization process.

#### *4.2.2. Component-Level Partial Derivatives*

Improvements in computational efficiency are key to a successful MDAO framework. When treating the system model as a single analysis tool (tip-to-tail), any change in the design variables necessitates re-analyzing the entire system. For example, in a single tip-to-tail approach, calculating the sensitivity of the vehicle forces to the nozzle aft length (design variable $\theta_{12} = L_8$, Table 1), requires the evaluation of a full system adjoint or re-simulation of the entire system at a perturbed state when using finite differences. Both necessitate "expensive" high-fidelity full-system simulations that include expensive to-evaluate sub-systems, such as the combustion chamber. Meanwhile, a modular approach allows the nozzle and aerodynamic components to be analyzed without the need to re-simulate the entire system, by propagating the partial derivatives introduced in Eq. 10 between sub-systems.

The modular plus partial derivative approach provides significant additional merit. Utilizing partial derivatives and the chain rule, designers can easily observe how states in the system affect sub-system performance, and vice versa, how changes in sub-system design impacts system performance. For example, when designing the inlet ramps and cowl, the aerodynamics engineer's interface is the flow state and geometry of the inlet throat ①. Combining the expected change in this flow state, $\vec{g}^I$ (or associated fluxes, $\vec{f}^I$) with partial derivatives of engine and nozzle performance with respect to this flow state, the effect of the proposed change on the vehicle thrust (and overall performance) can be estimated easily and quickly, without the need to involve any other design groups. If desirable, the current approach could be expanded to replace the STA quasi-constant values at the interfaces with parametrically defined profiles.

#### *4.2.3. Model Limitations*

As demonstrated in Section 4.1, good agreement was realized between the low-order analysis tools developed and a higher-fidelity CFD solver. However, in its current state of development, modeling assumptions underlying the `HyperPro` analysis tool pose limitations to the physical phenomena simulated. Caution should be exercised in drawing design conclusions for "real-life" problems. Some of these assumptions and their implications were discussed previously (inlet shock-shock interaction, Section 4.2.1, and the 1-D STA assumption, Section 4.2.2). The following simplifications may limit the applicability of the current design tools.

(1) Viscous effects throughout the engine flow path are significant. Appropriate treatment of their contribution to drag and how they affect propulsion performance is required.

(2) The engine performance is highly sensitive to the combustion process characteristics and efficiency. While appropriate source terms can capture the performance of a combustor, currently there is no suitable tool to set these.

(3) 3-D effects on a vehicle-integrated inlet are important for achieving vehicle design closure (aerodynamics - propulsion - control - weight and balance design).

#### *4.2.4. Future Work*

`HyperPro` as presented serves as a proof of concept for the methods discussed above. Further improvements to the framework described in Section 4.2.3 are planned. The modular analysis method and the underlying design tools will enable vehicle optimization (single point) and Co-design system-level MDAO problems to be explored efficiently. The effect of executing trajectory optimization in parallel to the vehicle design optimization will be realized. Research questions such as proper objective function formulation and its effect on the optimized system will be explored.

The developed framework can provide insight into the sensitivity of the system performance to component-level characteristics, thus laying out a road map to the most significant elements of the models that should be improved upon.

## 5. Conclusions

An efficient method for calculating a scramjet-propelled hypersonic vehicle's aerodynamic and propulsion system sensitivities to its geometry and control design variables was developed. A modular component-based modeling approach was developed for analyzing the nominal characteristics of the vehicle as well as calculating the system sensitivity matrix (Jacobian), $\frac{d\vec{F}}{d\vec{\theta}}$.

The newly developed propulsion analysis tool `HyperPro` is capable of 2-D forebody (inlet) and cowl analysis and 1-D isolator-engine analysis. As part of the vehicle analysis process, it provides: (1) combustion chamber outflow conditions, (2) propulsion system forces, and (3) sensitivities of outflow conditions and forces to geometry design variables and propulsion system control variables. Nozzle performance and sensitivities are evaluated using the aerodynamic sensitivity analysis tool `PySAGAS`, which was updated to allow propagation of inflow sensitivities (see Section 3.5.1). The full vehicle forces Jacobian matrix is constructed by chaining all component sensitivities (partial derivatives) together.

The proof of concept low-fidelity Inlet-Cowl-Combustor model proved adequate when compared with a 2-D inviscid CFD solver (`Puffin`). Similarly, the validity of the sensitivity calculation method and the modular approach for calculating the overall vehicle derivatives was demonstrated. Following this approach, the efficiency gain in calculating the vehicle's sensitivities is twofold: First, the analytic nozzle sensitivity calculation can be applied to a high-fidelity base flow (nominal) solution. Thus, a high-quality objective function evaluation (for optimization problems) is augmented with a computationally cheap Jacobian matrix. Second, calculating the partial derivative (or derivatives of parts of the whole system) is often more efficient than calculating the full derivative of the system as a whole. Furthermore, the use of partial derivatives can provide system-level insights into the component-level design process.

The advantages described above may be invaluable when performing a system-level MDAO study. Achieving optimal mission performance objectives, by combining the vehicle shape and propulsion optimization with trajectory optimization, dictates the need to optimize over a large number of design variables. Efficient means of obtaining the system sensitivities with sufficient accuracy are highly sought-after. At the conceptual design phase, the ability to individually analyze a single component's effect on the system's performance, and vice versa is also well appreciated. Further development of `HyperPro` analysis tool, for a better yet still computationally cheap representation of the engine's physics is planned. Integration of the full vehicle analysis tool into a vehicle, and Co-design (vehicle and trajectory) optimization framework will follow thereafter.

## References

[1] B. G. Coulter, D. Huang, and Z. Wang, "Geometric design of hypersonic vehicles for optimal mission performance with high-fidelity aerodynamic models," *Journal of Aircraft*, pp. 1–13, Nov. 2022. DOI: 10.2514/1.c036980.

[2] K. Bowcutt, G. Kuruvila, T. Grandine, and E. Cramer, "Advancements in multidisciplinary design optimization applied to hypersonic vehicles to achieve performance closure," American Institute of Aeronautics and Astronautics, Apr. 2008, ISBN: 978-1-60086-985-3. DOI: 10.2514/6.2008-2591. [Online]. Available: https://arc.aiaa.org/doi/10.2514/6.2008-2591.

[3] K. G. Bowcutt, "Multidisciplinary optimization of airbreathing hypersonic vehicles," *Journal of Propulsion and Power*, vol. 17, pp. 1184–1190, 6 2001, ISSN: 15333876. DOI: 10.2514/2.5893.

[4] N. Morita, T. Tsuchiya, and H. Taguchi, "{Mdo} of hypersonic waverider with trajectory-aero-structure coupling," American Institute of Aeronautics and Astronautics Inc, AIAA, 2020, ISBN: 9781624106002. DOI: 10.2514/6.2020-2402.

[5] J. R. R. A. Martins and S. A. Ning, *Engineering design optimization*. 2021, p. 637, ISBN: 9781108833417.
[6] K. Mackle and I. Jahn, "Efficient and flexible methodology for the aerodynamic shape optimization of hypersonic vehicle concepts in a high-dimensional design space," American Institute of Aeronautics and Astronautics (AIAA), Jan. 2024. DOI: 10.2514/6.2024-2838.
[7] P. A. Jacobs. "Gdtk." (), [Online]. Available: https://github.com/gdtk-uq/gdtk.
[8] T. Jazra, D. Preller, and M. K. Smart, "Design of an airbreathing second stage for a rocket-scramjet-rocket launch vehicle," *Journal of Spacecraft and Rockets*, vol. 50, pp. 411–422, 2 2013, ISSN: 15336794. DOI: 10.2514/1.A32381.
[9] D. Preller, "Multidisciplinary design and optimisation of a pitch trimmed hypersonic airbreathing accelerating vehicle," The University of Queensland, Apr. 2018. DOI: 10.14264/uql.2018.437.
[10] K. Mackle, A. Lock, I. Jahn, and C. van der Heide, "Developing a co-design framework for hypersonic vehicle aerodynamics and trajectory," American Institute of Aeronautics and Astronautics (AIAA), Jan. 2024. DOI: 10.2514/6.2024-0238.
[11] J. A. Andersson, J. Gillis, G. Horn, J. B. Rawlings, and M. Diehl, "Casadi: A software framework for nonlinear optimization and optimal control," *Mathematical Programming Computation*, vol. 11, pp. 1–36, 1 Mar. 2019, ISSN: 18672957. DOI: 10.1007/s12532-018-0139-4.
[12] K. A. Damm, R. J. Gollan, P. A. Jacobs, *et al.*, "Discrete adjoint optimization of a hypersonic inlet," *AIAA Journal*, vol. 58, pp. 2621–2634, 6 2020, ISSN: 00011452. DOI: 10.2514/1.J058913.
[13] J. D. Anderson, *Hypersonic and High-Temperature Gas Dynamics, Third Edition*. American Institute of Aeronautics and Astronautics, Inc., Mar. 2019, ISBN: 978-1-62410-514-2. DOI: 10.2514/4.105142. [Online]. Available: https://arc.aiaa.org/doi/book/10.2514/4.105142.
[14] W. Heiser, D. Pratt, D. Daley, and U. Mehta, *Hypersonic Airbreathing Propulsion*. American Institute of Aeronautics and Astronautics, Inc., Jan. 1994, ISBN: 978-1-56347-035-6. DOI: 10.2514/4.470356.
[15] I. H. Jahn, "Conceptual study into wave ingesting propulsion for hypersonic flight," American Institute of Aeronautics and Astronautics (AIAA), May 2023. DOI: 10.2514/6.2023-3034.
[16] D. Curran, V. Wheatley, and M. Smart, "Investigation of combustion mode control in a mach 8 shape-transitioning scramjet," *AIAA Journal*, vol. 57, pp. 2977–2988, 7 2019, ISSN: 1533385X. DOI: 10.2514/1.J057999.
[17] E. Arad, N. Yokev, H. E. Brod, and D. Michaels, "From supersonic combustion to thermal choking: Numerical and experimental analysis of a scramjet engine," vol. 1 PartF, American Institute of Aeronautics and Astronautics Inc, AIAA, 2020, ISBN: 9781624105982. DOI: 10.2514/6.2020-2966.
[18] M. Smart, "Scramjets," *Aeronautical Journal*, vol. 111, pp. 605–620, 1124 2007, ISSN: 00019240. DOI: 10.1017/s0001924000004796.
[19] M. K. Smart, "How much compression should a scramjet inlet do," *AIAA Jurnal*, vol. 50, 3 2012. DOI: 10.2514/1.J051281.
[20] P. P. Araújo, R. Y. Tanaka, C. A. Silva, A. Passaro, and P. G. Toro, "Multi-objective optimization of a hypersonic airbreathing vehicle," *Physics of Fluids*, vol. 36, 2 Feb. 2024, ISSN: 10897666. DOI: 10.1063/5.0181366.
[21] J. S. Robinson, "An overview of nasa's integrated design and engineering analysis (idea) environment," 2011, ISBN: 9781600869426. DOI: 10.2514/6.2011-2392.
[22] P. A. Jacobs, R. J. Gollan, and I. Jahn, "Guide to the geometry package," The University of Queensland, 2022.
[23] A. Mittelman. "Hyperpro." (2024), [Online]. Available: https://github.com/amirmit/HyperPro.
[24] R. A. Baurle and R. L. Gaffney, "Extraction of one-dimensional flow properties from multidimensional data sets," *Journal of Propulsion and Power*, vol. 24, pp. 704–714, 4 2008, ISSN: 15333876. DOI: 10.2514/1.32074.
[25] M. D. V. DYKE, "First- and second-order theory of supersonic flow past bodies of revolution," *Journal of Spacecraft and Rockets*, vol. 40, pp. 1029–1047, 6 Nov. 2003, ISSN: 0022-4650. DOI: 10.2514/2.7049.